analytical chemistry

Article

pubs.acs.org/ac

Real Time Observation of the Formation of Hollow Nanostructures through Solid State Reactions

Huang-Yen Lai,[§,†] Chun-Wei Huang,[§,†] Chung-Hua Chiu,[§,†] Chun-Wen Wang,[§] Jui-Yuan Chen,[§] Yu-Ting Huang,[§] Kuo-Chang Lu,[‡] and Wen-Wei Wu*[,§]

[§]Department of Materials Science and Engineering, National Chiao Tung University, No. 1001, University Rd, East Dist., Hsinchu City, 300, Taiwan

[‡]Department of Materials Science and Engineering, National Cheng Kung University, Tainan, 701, Taiwan

Supporting Information

ABSTRACT: We demonstrate the formation of hollow nickel germanide nanostructures of Ni−Ge core−shell nanoparticles by solid state reactions. The structural evolutions of nickel germanide hollow nanostructures have been investigated in real-time ultrahigh vacuum transmission electron microscopy (UHV-TEM). Annealed above 450 °C, the nonequilibrium interdiffusion of core and shell species occurred at the interface; thus, Ni germanide hollow nanostructures were formed by solid state reactions involving the Kirkendall effect. In addition, the different hollow nanostructures formed from different core diameters of Ni−Ge core−shell nanoparticles have been studied. Also, we propose the mechanism with effects of the size and annealing duration on the solid state reactions based on the Kirkendall effect.

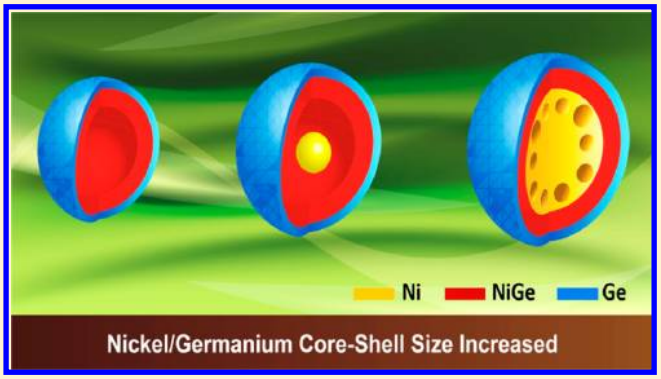

Over the past decade, hollow nanostructures have emerged as new functional materials and have attracted applications in high efficiency catalysis,[1−3] sensing,[4−6] lithium-ion batteries,[7−11] and biomedical science and engineering[12−16] due to their unique and novel structures, such as high surface-to-volume ratio and a large pore volume. There are many approaches commonly used to synthesize the hollow nanostructures, including template-mediated methods,[17−20] chemical etching,[21,22] and recently, galvanic replacement[23,24] and the nanoscale Kirkendall effect.[25−27] Among them, the nanoscale Kirkendall effect is almost through the solid−gas state system[25,28] and solid−liquid state system,[26,27] providing a novel and effective method to fabricate hollow nanostructures. In contrast, fabricating hollow nanostructures through solid−solid state reactions[29] is rare in related studies, which is attributed to the difficult preparation of the solid−solid state core−shell system with appropriate coating properties. Although transition metal-group IV compounds formation has been reported through the Kirkendall effect,[30] the reaction process of solid state reactions to form hollow nanostructures via the Kirkendall effect mechanism has never been observed directly, even including various assumptions during the actual reaction process. Therefore, the Ni−Ge system was used as the model system of extremely different interdiffusion rates between Ni and Ge, which is helpful for observing diffusion behaviors at the interface via the Kirkendall effect. Furthermore, the nickel germanide, the product of this system, exhibits many excellent properties, such as wide temperature stability, facile chemical processing, and low resistivity, having been demonstrated to be a promising Schottky barrier source/drain material in Ge-based p-channel metal oxide semiconductor field effect transistors (MOSFETs).[31−35] However, hollow nanostructures of nickel germanides have never been synthesized. In this work, the formation of hollow nickel germanide nanostructures by solid state reactions of Ni−Ge core−shell nanoparticles has been investigated. The different hollow nanostructures formed from different core diameters of Ni−Ge core−shell nanoparticles are discussed. Additionally, in situ transmission electron microscopy (TEM) is a powerful tool for atomic-level observation, including phase/shape transformations,[36−38] electron transport behaviors,[39−42] and solid−liquid interactions in wet cells.[43] Also, utilizing the in situ observation, the formation mechanism of hollow nanostructures has been demonstrated. Although the formation behavior can be driven by electron beam irradiation, it can be neglected in our case because we found that some core−shell structures successfully reacted to be yolk−shell structures without electron beam irradiation. This may enhance the applications in the fabrication of other nanosystems with different hollow morphologies based on the mechanism proposed in this study.

Received: January 12, 2014
Accepted: March 26, 2014
Published: March 26, 2014

   dx.doi.org/10.1021/ac500134u | *Anal. Chem.* 2014, 86, 4348−4353

EXPERIMENTAL SECTION

Ni−Ge core−shell nanoparticle arrays with various diameters and intervals were fabricated by utilizing an e-beam lithography (EBL) system and designed pattern on a Si_3N_4 membrane window grid. The process is shown in Figure S-1, Supporting Information. PMMA was coated on the Si_3N_4 membrane, and then, nanoparticle arrays were defined by e-beam lithography. After the development process, Ni film was deposited on the substrate by e-beam evaporator (EBE). Following the lift-off process in the acetone, the Ni nanoparticle arrays were prepared. Then, Ge film was deposited to cover the Ni nanoparticle arrays by EBE. A field emission scanning electron microscope (FESEM, JEOL JSM-6500F) was used to examine the morphology of core−shell nanoparticle arrays. High-resolution lattice imaging and line scan were performed by a high resolution transmission electron microscope (HRTEM, JEOL 2100F) equipped with an energy dispersive spectrometer (EDS). To observe diffusion behaviors at the interface between the core and shell, the cross-sectional sample of Ni−Ge core−shell nanoparticle was prepared with focused ion beam (FIB). The Ni−Ge core−shell nanoparticle capped with 100 nm-thick SiO_2 was fabricated on a Si_3N_4 membrane. The Pt and SiO_2 film typically deposited on the Ni−Ge core−shell nanoparticle was utilized to prevent the sample from ion beam sputtering damage and Pt diffusion during annealing, respectively. After that, the cross-sectional sample was then annealed and observed by in situ TEM. During the reaction, the temperature was raised to 450 °C to investigate the morphological and structural change of the Ni−Ge core−shell nanoparticle by solid state reactions via the Kirkendall effect.

RESULTS AND DISCUSSION

Figure 1a,b shows SEM images of Ni−Ge core−shell nanoparticle arrays fabricated by utilizing the e-beam lithography system and designed pattern. It can be clearly seen that the outer shell was coated over the inner core completely. Figure 1c presents a typical TEM image of a Ni−Ge core−shell nanoparticle; the strong contrast between the dark core and the relatively bright edge is evidenced by their compact contact. Notably, the diameter of the inner Ni nanoparticle is about 83 nm, and the thickness of the outer Ge shell is about 80 nm. Furthermore, the amorphous structure of the outer Ge shell results in their ambiguous contour indicated by dashed lines, while the inner Ni core has a polycrystalline structure. Figure 2b shows the TEM image of a Ni−NiGe yolk−shell nanostructure obtained during annealing at 450 °C for 30 min through the Kirkendall effect. As shown in Figure 1d, the inner Ni atoms diffused mostly into the outer Ge shell. The interior of the Ni−Ge core−shell generated a void of about 100 nm in diameter. It shows that around 50 nm of the inner Ni nanoparticle remained unreacted. The hollow sphere was found uniform, and the formed NiGe shell thickness was about 20−30 nm. Figure 1e,f shows HRTEM images of the Ni−NiGe yolk−shell nanostructure marked in Figure 1d, respectively. The lattice spacings of the shell are 0.249 and 0.191 nm, which correspond to $(1\bar{1}1)$ and (211) planes of the orthorhombic NiGe phase, and the angle between the planes is 84.96°. On the other hand, the lattice spacings of the yolk are 0.2046 and 0.2063 nm, corresponding to $(1\bar{1}1)$ and $(11\bar{1})$ planes of the cubic Ni phase, and the angle between the planes is 70.53°. In addition, NiGe phase can be formed through solid state reactions of Ge and Ni, which is highly attractive due to its low

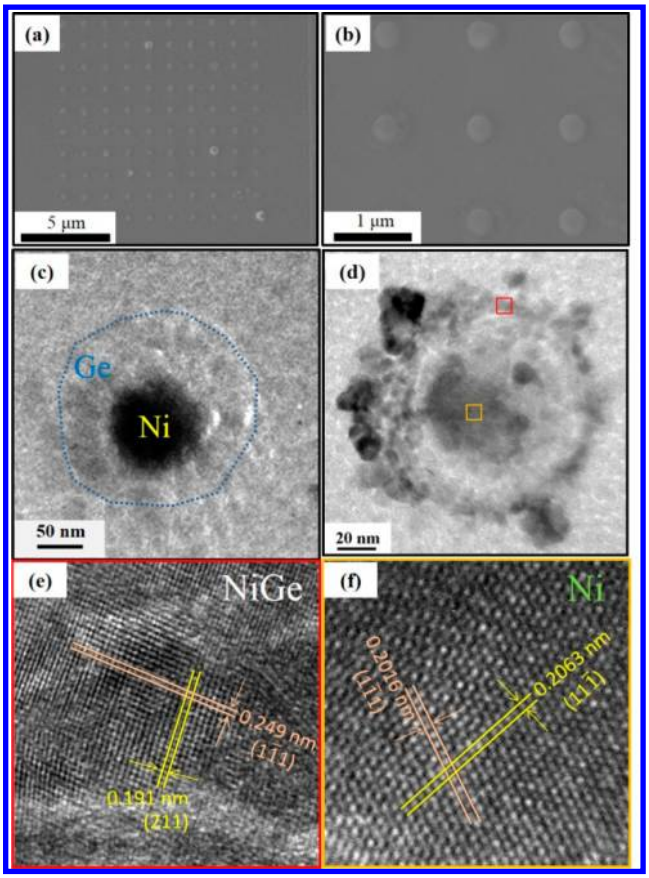

Figure 1. (a) and (b) Ni−Ge core−shell nanoparticles of different sizes fabricated on a Si_3N_4 membrane substrate. (c) TEM image of a Ni core covered by a Ge shell. (d) TEM image of a Ni−NiGe yolk−shell nanoparticle formed during annealing at 450 °C. (e) The HRTEM image of the NiGe shell. (f) The HRTEM image of the Ni core.

processing temperature of about 250 °C. In this study, the demand for the purpose of imaging the real time reaction process stimulated us to raise the reaction temperature up to 450 °C to decrease the reaction time although the NiGe can indeed react at low processing temperature of about 250 °C. Figure S-2a,c, Supporting Information, shows the TEM images and the related EDS spectra revealing the composition and structure of the Ni−NiGe yolk−shell nanostructure. The EDS line scan in Figure S-2b,d, Supporting Information, explicitly shows the compositional profile after the reaction. The intensity profile demonstrates the Ni−NiGe yolk−shell nanostructures and confirms the outward diffusion of Ni while Ge mostly remains, indicating that the partially hollow interior has been formed via the Kirkendall effect. In addition, EDS mapping of Ni−NiGe yolk−shell nanoparticle has further confirmed this viewpoint in Figure S-2e, Supporting Information. Figure 2a−c shows the TEM images of Ni−Ge core−shell nanoparticles during the same reaction condition, annealing at 450 °C for 30 min via the Kirkendall effect, with core diameters of 50, 80, and 200 nm.

Comparing Figure 2a−c reveals that increasing the core diameter leads to a significant change in the morphologies of fully hollow structures, yolk−shell structures, and porous structures, respectively. Supporting video-1, ac500134u_si_002.avi, Supporting Information, shows the formation process of a Ni−NiGe yolk−shell nanostructure during

dx.doi.org/10.1021/ac500134u | Anal. Chem. 2014, 86, 4348−4353

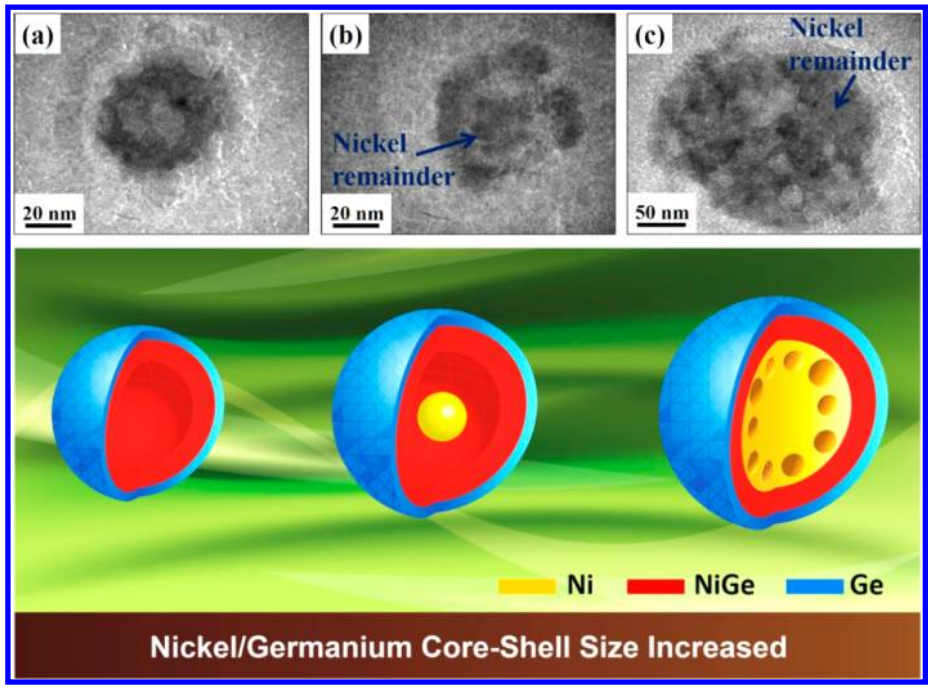

Figure 2. Different morphologies and structures of hollow nickel germanide nanoparticles with different core diameters; (a) fully formed hollow structure, (b) yolk–shell structure, and (c) porous structure.

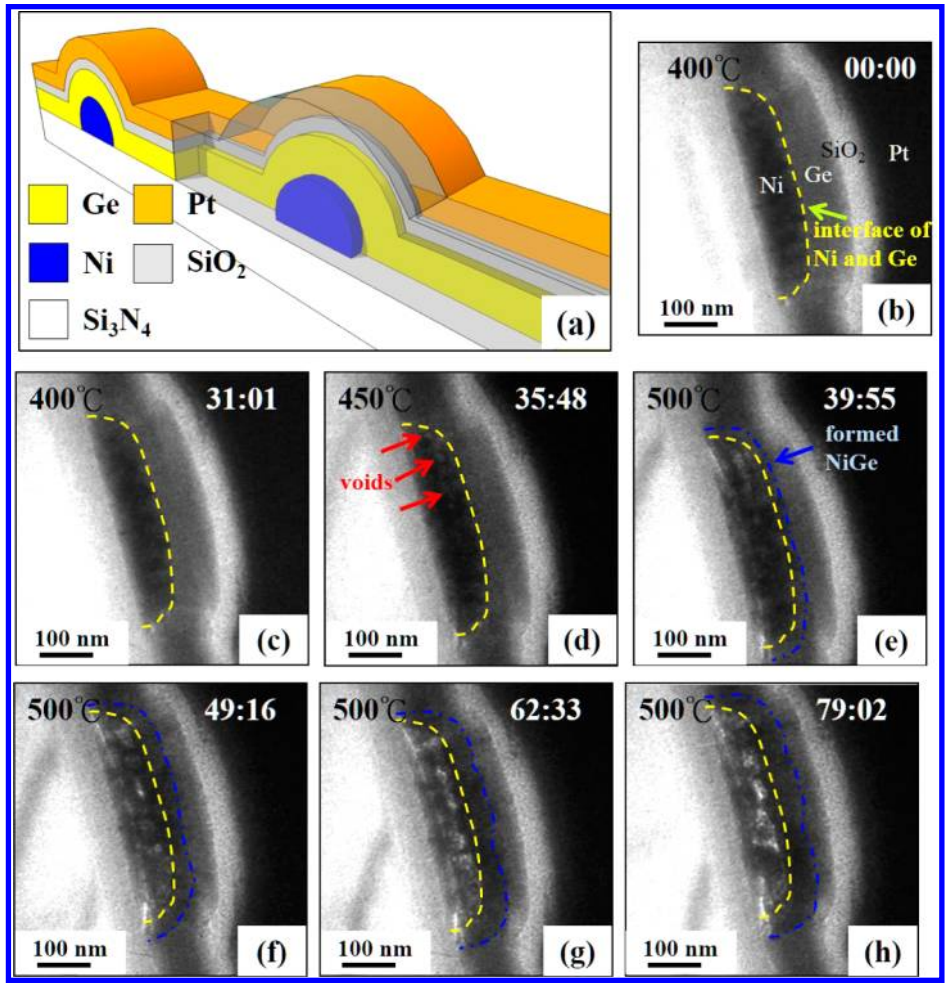

Figure 3. (a) Schematic illustration of a Ni–Ge core–shell cross-sectional FIB sample. (b)–(h) A time-resolved series of TEM images captured from an in situ TEM video, showing the void formation process of a Ni–Ge core–shell nanoparticle during annealing above 400 °C.

dx.doi.org/10.1021/ac500134u | *Anal. Chem.* 2014, 86, 4348–4353

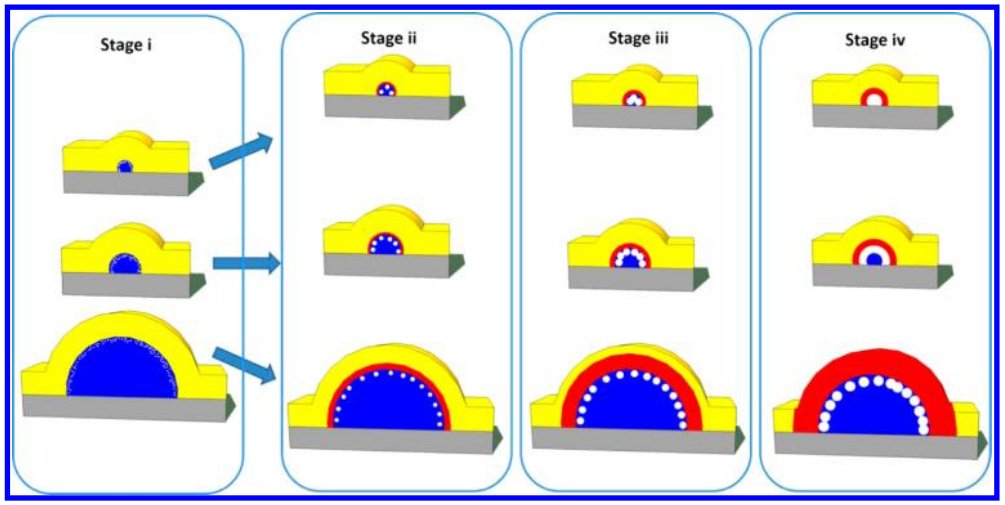

Figure 4. Schematic illustration of the hollow structures formed via the Kirkendall effect. Stage (i) Vacancies are formed through the nonequilibrium interdiffusion of core and shell species via the Kirkendall effect at specific temperatures. Stage (ii) Saturated vacancies agglomerate to form numerous voids by thermal vibration at specific temperatures, and the reactant is formed between the core and shell. Stage (iii) Voids grow gradually with agglomeration of adjacent small voids, which is influenced by the size of the core. Stage (iv) With the size effect, different nanostructures are formed.

annealing at 450 °C. A similar behavior about covered shells of different core diameters to form hollow nanostructures of different morphologies was discussed from the oxidation of Ni nanoparticles.[44] During the treatment at 500 °C for 2 h, the Ni nanoparticles with 96 nm diameter were formed to be Ni−NiO porous nanostructures rather than a large void within hollow nanostructures of Ni nanoparticles with diameters below 26 nm heated at 300 °C for 2 h.

Furthermore, in order to directly observe the atomic interdiffusion behavior at the interface between the core, shell, and the formed reactant movement profile via the Kirkendall effect, the cross-sectional sample of Ni−Ge core−shell nanoparticle was prepared with FIB as illustrated in Figure 3. The schematic illustration of the cross-sectional FIB sample is shown in Figure 3a, and each component is labeled accordingly. Figure 3b−h is captured from an in situ TEM video, revealing the Kirkendall voids and yolk−shell Ni−NiGe nanostructure. Figure 3b shows the cross-sectional TEM image of the Ni−Ge core−shell nanoparticle before annealing. The yellow dash line denotes the interface between Ni and Ge. Figure 3c shows the cross-sectional TEM image during annealing at 400 °C for about 30 min as the voids and reactant were not found. This may be attributed to the slow interdiffusion rates of Ni and Ge at 400 °C. When the temperature ramped to 450 °C, several small voids of about 6−7 nm in dimension clearly appeared in Figure 3d, formed within the Ni near the original interface during annealing for less than 5 min. The result indicates that Ni has a faster diffusion rate than Ge. However, neither the contrast of the reactant nor the interface movement between Ni and the reactant can be clearly observed. Figure 3e shows the cross-sectional TEM image of the sample as ramped to 500 °C for about 4 min with the faster diffusion of Ni outward; some voids begin to grow gradually with consumption of adjacent smaller voids. We propose that the thermodynamic driving force of the phenomenon is to reduce the surface energy through agglomeration of adjacent small voids. In addition, the contrast of the reactant appeared between the original interface and outer Ge. Figure 3f shows the cross-sectional TEM image of the sample annealed at 500 °C for over 10 min. We can see that these large voids of about 15 nm in dimension grew continuously within the Ni near the original interface, and the thickness of the formed NiGe shell was about 40 nm. When the sample was annealed at 500 °C for 25 min, these large voids grew until they connected with each other as shown in Figure 3g. During the diffusion process, inner nickel atoms diffused outward into the outer germanium shell only through a small number of connected regions. Figure 3h shows the cross-sectional TEM image of the sample annealed at 500 °C for 40 min. Notably, the thickness of the formed NiGe shell was about 45 nm and hardly thickened, resulting from the fact that excess nickel atoms were almost isolated by these voids near the original interface; thus, they were unable to diffuse outward. This was probably the reason why the yolk−shell nanostructure formed during the reaction. Additionally, this initial interface marked by yellow dash contour is likely to be pinned at the original location in our model system, probably resulting from the effect that, while Ni atoms diffuse outward to the outer germanium shell, the accompanied voids would tend to agglomerate adjacent small voids into a larger one with low mobility. Though this behavior is attributed to reducing the surface energy, the voids agglomeration has particular saturation that prevents them from opposite diffusion to the initial interface, indicative of the negligible movement of the mark interface, as displayed in Figure 3. Additionally, we noted that the solid state reaction between Ni−Ge core−shell systems may occur uniformly around the Ni−a-Ge interface instead of the heterogeneous boundary among Ni core, Ge shell, and nitride membrane with relatively high energy in our case. On the other hand, there were many vacancies inside a-Ge layer with much larger surface energy than that of the heterogeneous boundary at the reaction temperature. As a result, we propose that the main driving force of the outward diffusion of Ni atoms to Ge shell is likely the reduction in energy by mixing the two atoms into chemical compound, which is associated with the increase in the entropy of the Ni−Ge core−shell nanostructure as the Kirkendall effect.

A schematic illustration depicting the solid state reaction process of Ni−Ge core−shell with different sizes via the Kirkendall effect is presented in Figure 4. The mechanism is mainly divided into four stages: (i) Vacancies are formed through the nonequilibrium interdiffusion of core and shell species via the Kirkendall effect at specific temperatures. (ii)

dx.doi.org/10.1021/ac500134u | Anal. Chem. 2014, 86, 4348−4353

Saturated vacancies agglomerate to form numerous voids by thermal vibration at specific temperatures, and the reactant is formed between the core and shell. (iii) Voids grow gradually with agglomeration of adjacent small voids, which is influenced by the size of the core. (iv) With the size effect, different nanostructures are formed.

In stage (i) and stage (ii), core−shell nanoparticles with small, medium, and large core sizes undergo the same reaction where small voids are formed at the interface between the core and shell by saturated vacancies via the Kirkendall effect. In stage (iii) and stage (iv), for core−shell nanoparticles with a small core size, the small voids grow into a larger void. Eventually, the hollow nanostructure is formed. For core−shell nanoparticles with a medium core size, the voids grow but the core atoms cannot diffuse outward since the core is separated by the voids near the interface so that the yolk−shell nanostructure is formed. On the other hand, for core−shell nanoparticles with a large core size, the voids grow and there are sufficient core atoms diffusing outward; however, the original shell has formed to be the reactant entirely so that the diffusion behavior is interrupted and porous nanostructures appear.

CONCLUSIONS

In summary, the Ni−NiGe yolk−shell nanostructure has been formed from as-fabricated controllable Ni−Ge core−shell nanoparticles during annealing at 450 °C via the Kirkendall effect. With in situ TEM, the formation of Ni−NiGe yolk−shell nanostructures by solid state reactions has been observed directly. During the reactions, voids were formed within the Ni near the interface, and the remaining inner nickel was almost isolated to be a Ni−NiGe yolk−shell nanostructure. Moreover, nanostructures of different morphologies were formed, including fully hollow, yolk−shell, and porous nanostructures from Ni−Ge core−shell nanoparticles of different core sizes. Also, we have proposed the mechanisms of the solid state reaction process for the Ni−Ge core−shell nanostructures of different dimensions. The unique hollow nanostructures may be applied as new functional materials in high efficiency catalysis, sensing, and drug delivery.

ASSOCIATED CONTENT

Supporting Information

Schematic illustration of the fabrication process of Ni−Ge core−shell nanoparticles, EDS line scan of the Ni−NiGe yolk−shell nanostructure, and two in situ TEM videos. This material is available free of charge via the Internet at http://pubs.acs.org.

AUTHOR INFORMATION

Corresponding Author

*E-mail: wwwu@mail.nctu.edu.tw.

Author Contributions

†H.-Y.L., C.-W.H., and C.-H.C. contributed equally

Notes

The authors declare no competing financial interest.

ACKNOWLEDGMENTS

W.-W.W. and K.-C.L. acknowledge the support by National Science Council through Grants NSC 102-2221-E-009-039, NSC 100-2628-E-009-023-MY3, and NSC 102-2221-E-006-077-MY3.

REFERENCES

(1) Li, H.; Bian, Z.; Zhu, J.; Zhang, D.; Li, G.; Huo, Y.; Li, H.; Lu, Y. *J. Am. Chem. Soc.* **2007**, *129* (27), 8406−8407.
(2) Zeng, Y.; Wang, X.; Wang, H.; Dong, Y.; Ma, Y.; Yao, J. *Chem. Commun.* **2010**, *46* (24), 4312−4314.
(3) Cao, S.-W.; Zhu, Y.-J. *J. Phys. Chem. C* **2008**, *112* (16), 6253−6257.
(4) Zhang, H.; Zhu, Q.; Zhang, Y.; Wang, Y.; Zhao, L.; Yu, B. *Adv. Funct. Mater.* **2007**, *17* (15), 2766−2771.
(5) Zhao, Q.; Gao, Y.; Bai, X.; Wu, C.; Xie, Y. *Eur. J. Inorg. Chem.* **2006**, *2006* (8), 1643−1648.
(6) Lou, X. W.; Wang, Y.; Yuan, C.; Lee, J. Y.; Archer, L. A. *Adv. Mater.* **2006**, *18* (17), 2325−2329.
(7) Poizot, P.; Laruelle, S.; Grugeon, S.; Dupont, L.; Tarascon, J. M. *Nature* **2000**, *407* (6803), 496−499.
(8) Lou, X. W.; Deng, D.; Lee, J. Y.; Archer, L. A. *Chem. Mater.* **2008**, *20* (20), 6562−6566.
(9) Ma, H.; Cheng, F.; Chen, J. Y.; Zhao, J. Z.; Li, C. S.; Tao, Z. L.; Liang, J. *Adv. Mater.* **2007**, *19* (22), 4067−4070.
(10) Arico, A. S.; Bruce, P.; Scrosati, B.; Tarascon, J.-M.; van Schalkwijk, W. *Nat. Mater.* **2005**, *4* (5), 366−377.
(11) Wang, X.; Wu, X.-L.; Guo, Y.-G.; Zhong, Y.; Cao, X.; Ma, Y.; Yao, J. *Adv. Funct. Mater.* **2010**, *20* (10), 1680−1686.
(12) Skrabalak, S. E.; Chen, J.; Au, L.; Lu, X.; Li, X.; Xia, Y. *Adv. Mater.* **2007**, *19* (20), 3177−3184.
(13) Chen, J.-F.; Ding, H.-M.; Wang, J.-X.; Shao, L. *Biomaterials* **2004**, *25* (4), 723−727.
(14) Zhou, J.; Wu, W.; Caruntu, D.; Yu, M. H.; Martin, A.; Chen, J. F.; O'Connor, C. J.; Zhou, W. L. *J. Phys. Chem. C* **2007**, *111* (47), 17473−17477.
(15) Sokolova, V.; Epple, M. *Angew. Chem., Int. Ed.* **2008**, *47* (8), 1382−1395.
(16) Wei, W.; Ma, G.-H.; Hu, G.; Yu, D.; McLeish, T.; Su, Z.-G.; Shen, Z.-Y. *J. Am. Chem. Soc.* **2008**, *130* (47), 15808−15810.
(17) Caruso, F.; Caruso, R. A.; Möhwald, H. *Science* **1998**, *282* (5391), 1111−1114.
(18) Kim, S.-W.; Kim, M.; Lee, W. Y.; Hyeon, T. *J. Am. Chem. Soc.* **2002**, *124* (26), 7642−7643.
(19) Imhof, A. *Langmuir* **2001**, *17* (12), 3579−3585.
(20) Bao, J.; Liang, Y.; Xu, Z.; Si, L. *Adv. Mater.* **2003**, *15* (21), 1832−1835.
(21) Kim, D.; Park, J.; An, K.; Yang, N.-K.; Park, J.-G.; Hyeon, T. *J. Am. Chem. Soc.* **2007**, *129* (18), 5812−5813.
(22) Xiong, Y.; Wiley, B.; Chen, J.; Li, Z. Y.; Yin, Y.; Xia, Y. *Angew. Chem., Int. Ed. Engl.* **2005**, *44* (48), 7913−7917.
(23) Sun, Y.; Xia, Y. *Science* **2002**, *298* (5601), 2176−2179.
(24) Sun, Y.; Mayers, B.; Xia, Y. *Adv. Mater.* **2003**, *15* (7−8), 641−646.
(25) Cabot, A.; Puntes, V. F.; Shevchenko, E.; Yin, Y.; Balcells, L.; Marcus, M. A.; Hughes, S. M.; Alivisatos, A. P. *J. Am. Chem. Soc.* **2007**, *129* (34), 10358−10360.
(26) Yin, Y.; Erdonmez, C. K.; Cabot, A.; Hughes, S.; Alivisatos, A. P. *Adv. Funct. Mater.* **2006**, *16* (11), 1389−1399.
(27) Yin, Y.; Rioux, R. M.; Erdonmez, C. K.; Hughes, S.; Somorjai, G. A.; Alivisatos, A. P. *Science* **2004**, *304* (5671), 711−714.
(28) Peng, S.; Sun, S. *Angew. Chem., Int. Ed.* **2007**, *46* (22), 4155−4158.
(29) Fan, H. J.; Knez, M.; Scholz, R.; Nielsch, K.; Pippel, E.; Hesse, D.; Zacharias, M.; Gosele, U. *Nat. Mater.* **2006**, *5* (8), 627−631.
(30) Higgin, J. M.; Carmichael, P.; Schmitt, A. L.; Lee, S.; Degrave, J. P.; Jin, S. *ACS Nano* **2011**, *5*, 3268−3277.
(31) Gaudet, S.; Detavernier, C.; Kellock, A. J.; Desjardins, P.; Lavoie, C. *J. Vac. Sci. Technol., A: Vac., Surf., Films* **2006**, *24* (3), 474−485.
(32) Spann, J. Y.; Anderson, R. A.; Thornton, T. J.; Harris, G.; Thomas, S. G.; Tracy, C. *Electron Device Lett.* **2005**, *26* (3), 151−153.
(33) Brunco, D. P.; De Jaeger, B.; Eneman, G.; Mitard, J.; Hellings, G.; Satta, A.; Terzieva, V.; Souriau, L.; Leys, F. E.; Pourtois, G.; Houssa, M.; Winderickx, G.; Vrancken, E.; Sioncke, S.; Opsomer, K.; Nicholas, G.; Caymax, M.; Stesmans, A.; Van Steenbergen, J.; Mertens,

P. W.; Meuris, M.; Heyns, M. M. *J. Electrochem. Soc.* **2008**, *155* (7), H552−H561.
(34) Yan, C.; Higgins, J. M.; Faber, M. S.; Lee, P. S.; Jin, S. *ACS Nano* **2011**, *5* (6), 5006−5014.
(35) Zaima, S.; Nakatsuka, O.; Kondo, H.; Sakashita, M.; Sakai, A.; Ogawa, M. *Thin Solid Films* **2008**, *517* (1), 80−83.
(36) Hsin, C. L.; Lee, W. F.; Huang, C. T.; Huang, C. W.; Wu, W. W.; Chen, L. J. *Nano Lett.* **2011**, *11*, 4348−4351.
(37) Chiu, C. H.; Huang, C. H.; Chen, J. Y.; Huang, Y. T.; Hu, J. C.; Chen, L. T.; Hsin, C. L.; Wu, W. W. *Nanoscale* **2013**, *5*, 5086−5092.
(38) Huang, C. W.; Hsin, C. L.; Wang, C. W.; Chu, F. H.; Kao, C. Y.; Chen, J. Y.; Huang, Y. T.; Lu, K. C.; Wu, W. W.; Chen, L. J. *Nanoscale* **2012**, *4*, 4702−4706.
(39) Chen, J. Y.; Hsin, C. L.; Huang, C. W.; Chiu, C. H.; Huang, Y. T.; Lin, S. J.; Wu, W. W.; Chen, L. J. *Nano Lett.* **2013**, *13*, 3671−3677.
(40) Huang, Y. T.; Yu, S. Y.; Hsin, C. L.; Huang, C. W.; Kang, C. F.; Chu, F. H.; Chen, J. Y.; Hu, J. C.; Chen, L. T.; He, J. H.; Wu, W. W. *Anal. Chem.* **2013**, *85*, 3955−3960.
(41) Lee, K. Y.; Liew, S. L.; Chua, S. J.; Chi, D. Z.; Sun, H. P.; Pan, X. Q. *Mater. Res. Soc. Symp. Proc.* **2004**, *55*, 810−815.
(42) Tang, J.; Wang, C.-Y.; Xiu, F.; Lang, M.; Chu, L.-W.; Tsai, C.-J.; Chueh, Y.-L.; Chen, L.-J.; Wang, K. L. *ACS Nano* **2011**, *5* (7), 6008−6015.
(43) Miu, K. Y.; Park, J.; Zheng, H.; Alivisator, A. P. *Nano Lett.* **2013**, *13*, 5715−5719.
(44) Railsback, J. G.; Peck, A. C.; Wang, J.; Tracy, J. B. *ACS Nano* **2011**, *4*, 1913−1920.